Journal of Alloys and Compounds 522 (2012) 136–140

Contents lists available at SciVerse ScienceDirect

Journal of Alloys and Compounds

journal homepage: www.elsevier.com/locate/jallcom

Influence of Al content on martensitic transformation behavior in $Zr_{50}Cu_{50-x}Al_x$

F.Q. Meng[a,b,*], K. Tsuchiya[a,b], F.X. Yin[a], S. Ii[a], Y. Yokoyama[c]

[a] National Institute for Materials Science, Tsukuba, Ibaraki 305-0047, Japan
[b] University of Tsukuba, Tsukuba, Ibaraki 305-8577, Japan
[c] Tohoku University, Sendai, Miyagi 980-8577, Japan

ARTICLE INFO

Article history:
Received 11 November 2011
Received in revised form 10 January 2012
Accepted 22 January 2012
Available online 1 February 2012

Keywords:
Glasses
Metallic
Martensitic transformation
Thermal stability
Martensitic structure
Calorimetry

ABSTRACT

Influence of Al content on martensitic transformation temperature in ZrCu phase was investigated by differential scanning calorimetry for a series of $Zr_{50}Cu_{50-x}Al_x$ alloys. The crystallographic structure of the martensite was predominantly a monoclinic Cm, which is a superstructure of B19′. Microstructural observations revealed that a higher Al content above 6 mol% led to a pronounced formation of Zr_2Cu and τ_5 phases forming complex eutectic microstructures. The electron probe microanalysis indicated that the Al atoms in ZrCu phase substitute the Cu atoms up to 6 mol% and the excess Al atoms exist mainly in the τ_5 phase. The increasing Al content from 0 to 6 mol% induced a decrease in the martensitic transformation start temperature, M_s, from 446 K to 311 K, and in the reverse martensitic transformation start temperature, A_s, from 537 K to 468 K. But M_s remained almost constant when the Al content is over 6 mol%. Thus, the substitution of the Cu atoms by the Al atoms in ZrCu phase led to the decrease in M_s and A_s.

1. Introduction

Structure and phase transformation in binary ZrCu intermetallic compound has been studied since the early 1980s [1–5]. ZrCu exhibits two unique characteristics, namely martensitic transformation and high stability of amorphous phase. Koval et al. [6–8] reported that the equiatomic ZrCu intermetallic compound undergoes martensitic transformation (MT) from the cubic B2 structure to two monoclinic martensite phases at 443 K [9], one with a base structure (B19′) with $P2_1/m$ symmetry and the other with its superstructure with Cm symmetry. Shape memory effect associated with the MT has been also observed [9–11].

On the other hands, relatively high glass-forming ability (GFA) in the ZrCu based alloy systems was demonstrated by Inoue et al. [12,13]. The addition of Al significantly improves the GFA with the maximum ΔT_x ($\Delta T_x = T_x - T_g$, T_g: glass transition temperature, T_x: onset temperature of crystallization) of 80 K at the composition of $Zr_{50}Cu_{40}Al_{10}$ [14]. Zr–Cu–Al bulk amorphous can be produced in the form of one centimeter diameter rod [15]. More recently, Zr–Cu–Al metallic glasses (MG) were shown to exhibit pronounced work hardening when the B2 crystals of several hundred nanometers are present in the structure due to the stress-induced martensitic transformation [16–19]. These MG/B2 composites may be a potential method to improve the plasticity of bulk metallic glasses (BMGs) after further adjustment of the structures and MT [20]. For Zr–Cu–Al metallic glasses, the improvement of Al on the GFA has been confirmed by Xing et al. [21]; however, there are few reports about the effect of Al content on the MT behavior in ZrCu intermetallic compound.

In this study, the influence of substitution of Cu by Al on the martensitic transformation temperatures in $Zr_{50}Cu_{50-x}Al_x$ alloys was investigated. The microstructure, crystallographic structure and phase transformation behaviors are presented, and the factors influencing the variation in the transformation temperatures are also discussed.

2. Materials and methods

Ingots of $Zr_{50}Cu_{50-x}Al_x$ ($x = 0, 2, 4, 6, 8, 10$) were prepared by arc-melting the element metals of Zr, Cu and Al in an argon atmosphere. Hereafter, the sample with x mol% aluminum will be referred to as xAl. To maintain a low-oxygen concentration in the alloys, a high purity Zr with the oxygen content less than 0.05 at% was used. The mother ingots of the alloys were remelted at least three times in order to ensure the chemical homogeneity. In the 10Al alloy with the highest glass formability, amorphous phase was observed in the bottom part of the ingots. All the ingots were completely remelted, and cast into cylindrical rods with the diameter of 10 mm. The X-ray diffraction analysis of the as-cast samples revealed that 6Al, 8Al and 10Al alloys were fully amorphous. All the samples were crystallized at 1073 K for 72 h in a sealed quartz tube under an argon atmosphere, followed by water quenching. This treatment was also sufficient to crystallize the amorphous phase in the 6Al, 8Al and 10Al samples. Crystal structures of the samples were characterized by X-ray diffractometry (XRD) with a Cu-Kα radiation (40 kV–300 mA). Differential scanning calorimetry (DSC) was carried out using a TA Instrument DSC Q-10 with a heating/cooling rate of 0.17 K/s to determine the forward and reverse MT temperatures. All the DSC runs

* Corresponding author at: National Institute for Materials Science, Tsukuba, Ibaraki 305-0047, Japan.
E-mail address: meng.fanqiang@nims.go.jp (F.Q. Meng).

0925-8388/$ – see front matter © 2012 Elsevier B.V. All rights reserved.
doi:10.1016/j.jallcom.2012.01.125

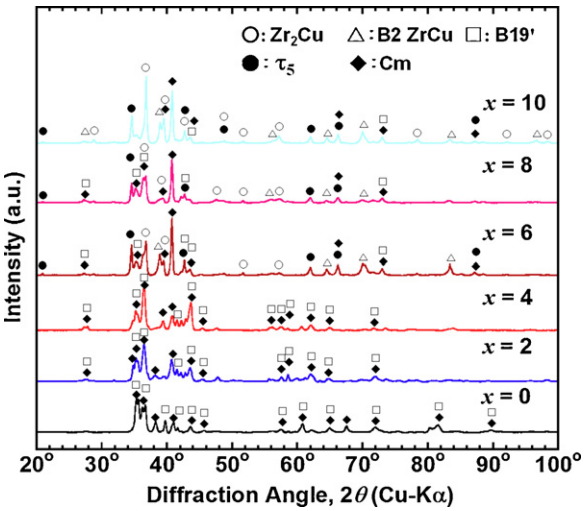

Fig. 1. X-ray diffraction patterns of $Zr_{50}Cu_{50-x}Al_x$ (x = 0, 2, 4, 6, 8, 10) after crystallization treatment at 1073 K for 72 h.

were started from a heating run after holding the samples at 193 K for 5 min. The microstructure was investigated by optical microscopy (OM) using a Nikon Eclipse LV150 microscope with a differential interference mode, and by backscattered electrons (BSE) mode on a JEOL 7001F scanning electron microscope (SEM), operated at 20 kV. Transmission electron microscopy (TEM) was performed on a JEOL JEM-2000FX transmission electron microscope operated at 200 kV. The samples for OM and SEM observations were mechanically polished using SiO_2 (0.06 μm) colloidal suspension. Disc samples (⌀3 mm) for TEM observations were mechanically thinned to 150 μm thick and then perforated by electropolishing using a Tenupol-5 with an electrolyte consisting of 20 vol% nitric acid and 80 vol% methanol at a temperature of 253 K. The chemical compositions of different phases were determined by an electron probe microanalyzer (EPMA) using JEOL JXM-8530F.

3. Results and discussion

Fig. 1 shows the XRD patterns of the $Zr_{50}Cu_{50-x}Al_x$ samples after crystallization treatment at 1073 K for 72 h. It can be seen that all the samples have been fully crystallized, and both B19′ and Cm martensite phases are detected in all the samples. For the x = 0 and 2 samples, all the peaks can be assigned to the B19′ or Cm martensite phases, and no other phase is detected. As seen in Fig. 1 most of the peaks for B19′ and Cm martensite phases overlap and there are only a few minor peaks that can be solely attributed to B19′ (such as those at around 42 degree in 0Al and 2Al samples).

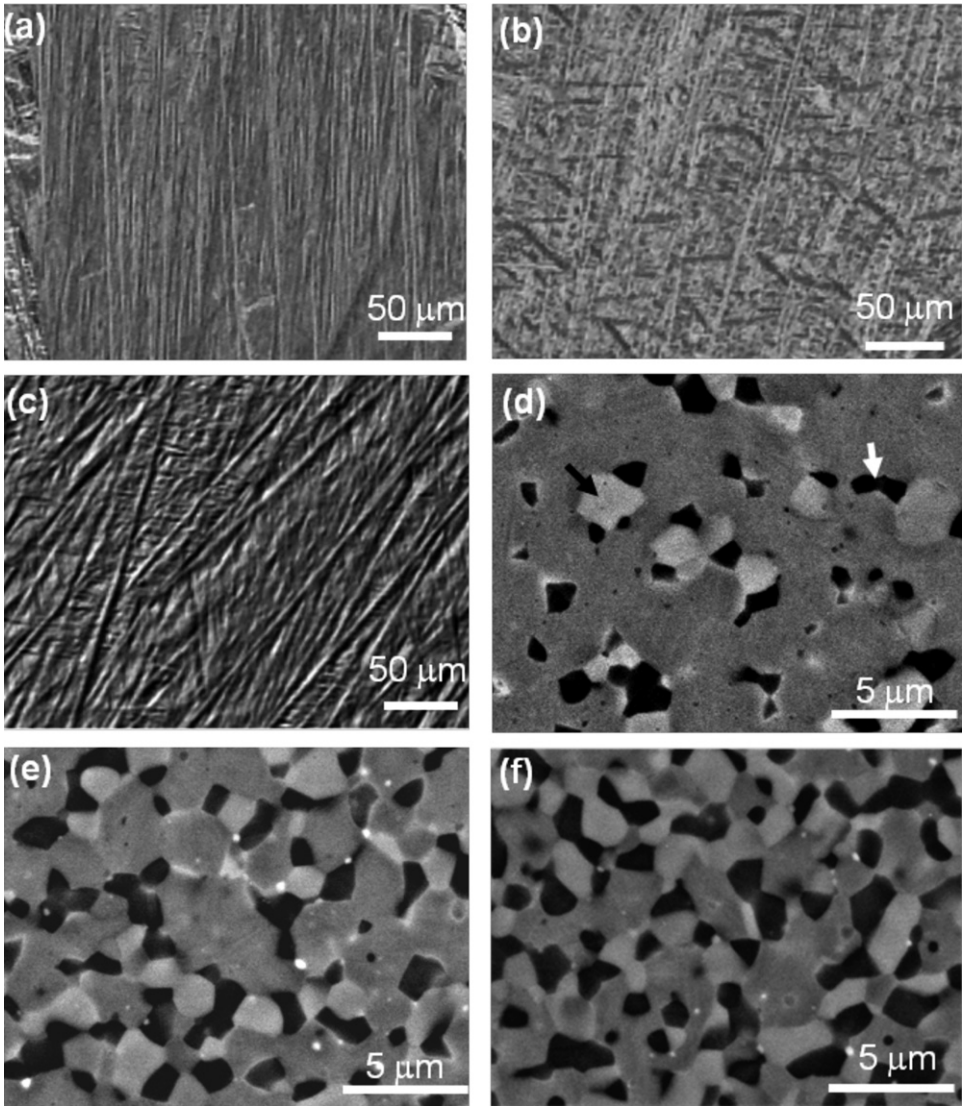

Fig. 2. Optical micrograph of (a) 0Al, (b) 2Al, (c) 4Al, and BSE-SEM micrographs of (d) 6Al, (e) 8Al, (f) 10Al after crystallization treatment at 1073 K for 72 h.

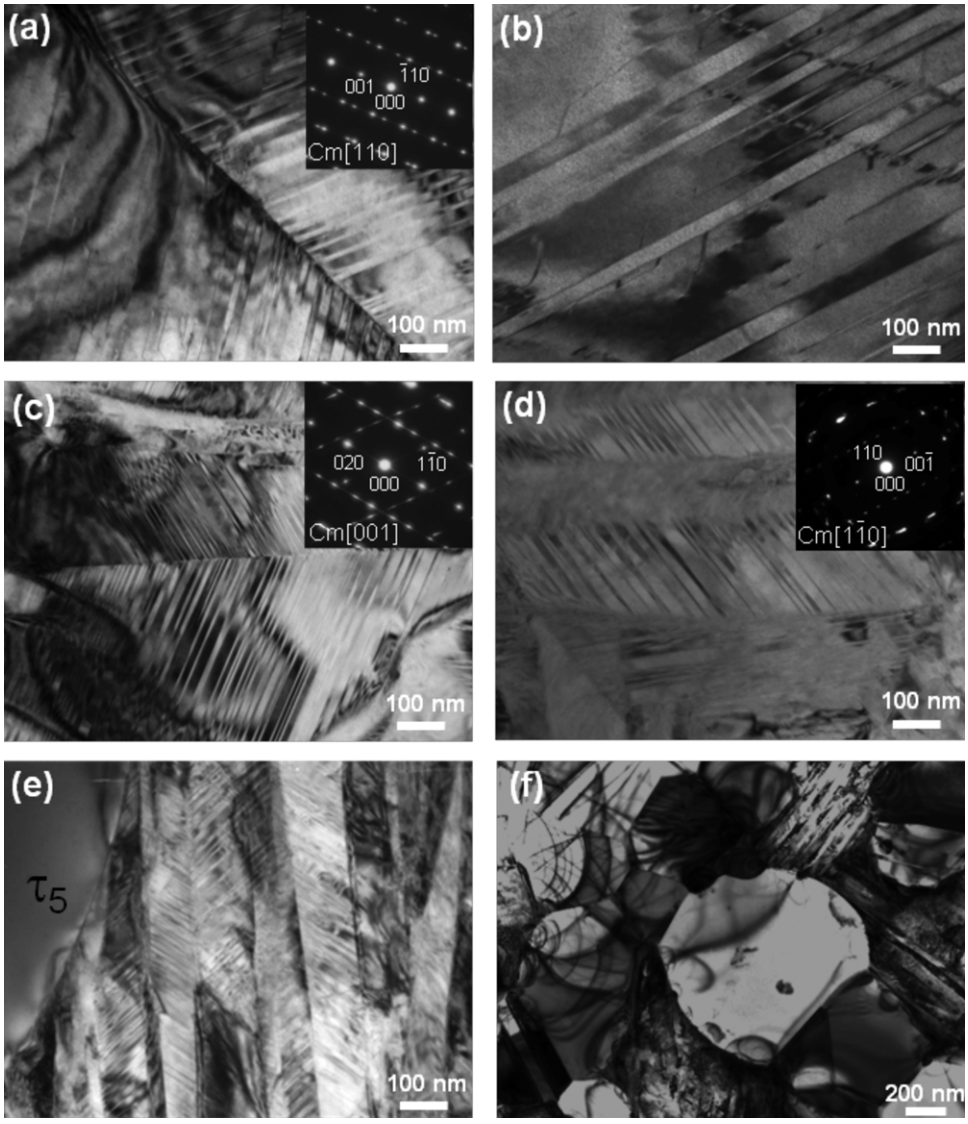

Fig. 3. TEM bright-field (BF) micrographs and selected area electron diffraction (SAED) patterns of $Zr_{50}Cu_{50-x}Al_x$: (a) 0Al, (b) 2Al, (c) 4Al, (d) 6Al, (e) 8Al, and (f) 10Al.

As shown later, TEM observations revealed that the Cm phase is the dominant martensite phase. Besides Cm and B19′ phases, B2 structure ZrCu phase is detected in 4Al. When the Al content is over 6 mol%, peaks of the ZrCu with B2 structure, Zr_2Cu with $C11_b$ structure and τ_5 with C15 structure phases are detected besides the martensite phases [22]. It can be seen from Fig. 1 that the intensity of B2 peak at diffraction angle of 39 degree becomes stronger as Al content increases from 4 to 8 mol%. As the x increases to 10 mol%, the intensity of B2 ZrCu peaks become weaker compared with 8Al sample; and the strongest peak corresponds to the Zr_2Cu phase. These results reveal that the B2 ZrCu cannot transform to Cm or B19′ martensite phases completely in the samples with $x \geq 4$.

The OM and BSE-SEM micrographs of the crystallized samples are presented in Fig. 2. Fig. 2(a)–(c) is corresponded to the OM micrographs showing the typical morphology of martensite plates in 0Al, 2Al and 4Al, respectively, which is consistent with the XRD analysis in Fig. 1. Further increase in Al content ($x \geq 6$) drastically changes the microstructures. As shown in Fig. 2(d), bright and dark secondary phases formed as Al up to 6 mol%. The EPMA analysis revealed that the phase showing brighter contrast (such as the one denoted by the black arrow in Fig. 2(d)) is Zr_2Cu ($Zr_{63.3}Cu_{35.2}Al_{1.5}$), and the one showing darker contrast (denoted by the white arrow in Fig. 2(d)) is τ_5 phase ($Zr_{37}Cu_{39.7}Al_{23.3}$). The consecutive increase of Al addition from 6 to 10 mol% also induces the increase in the volume fraction of Zr_2Cu and τ_5 phases, especially in 10Al. Comparison of the microstructures and phase diagram reported in [23] suggests that the ZrCu phase solidifies first, and then Zr_2Cu and τ_5 forms by a eutectic reaction. The Al addition ($x \geq 6$) induces the decomposition of ZrCu phase during the heat treatment at 1073 K.

According to the phase diagram reported by Markiv et al. [23], the solubility limit of Al in the ZrCu phase is about ~5 mol% and it agrees with the microstructure change in this studies. When the Al content is lower than the solubility limit, the dominant phase is ZrCu martensite phases. An increase of Al addition over 6 mol% induces the excess of Al, and leads to the formation of Zr_2Cu and τ_5 phases. The EPMA analysis also indicated that the excess Al concentrates in τ_5 phase.

Fig. 3 shows the TEM bright-field (BF) micrographs and selected area electron diffraction (SAED) patterns of 0Al, 4Al and 6Al. Martensitic twin structures were observed in all the samples, and the SAED patterns indicate that the predominant martensite structure is Cm [8]. In 8Al and 10Al, other Zr_2Cu and τ_5 phases were also observed in TEM. Only small amount of martensite phases exists in 10Al due to the high volume fraction of Zr_2Cu and τ_5 phases, and

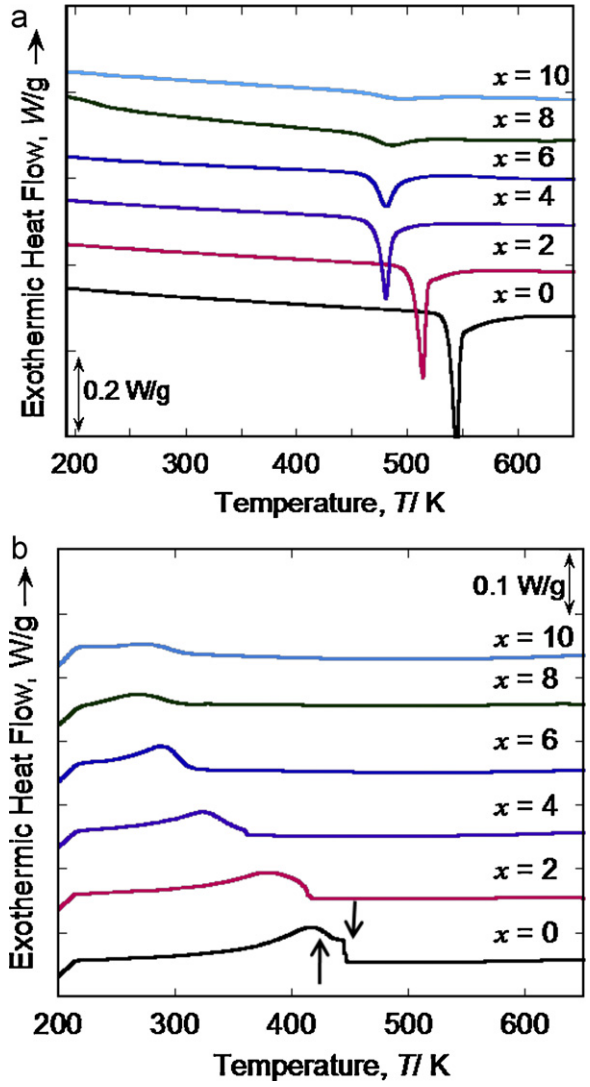

Fig. 4. Results of DSC measurements for $Zr_{50}Cu_{50-x}Al_x$ ($x = 0, 2, 4, 6, 8, 10$): (a) heating runs and (b) cooling runs.

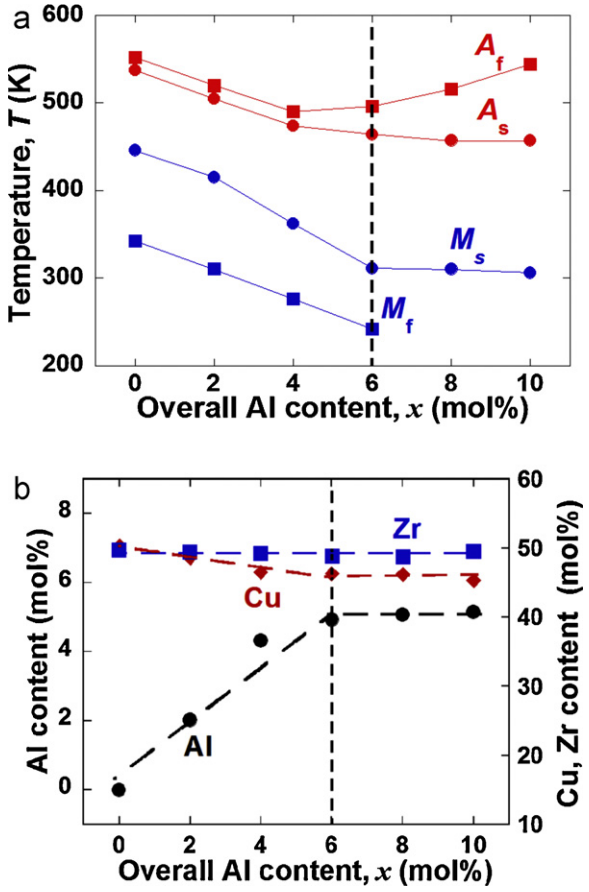

Fig. 5. (a) Change of forward and reverse martensitic transformation temperature M_s, M_f, A_s, and A_f in $Zr_{50}Cu_{50-x}Al_x$ after crystallization treatment at 1073 K for 72 h. (b) Chemical composition of the ZrCu phase plotted as a function of overall Al content.

planar faults, presumably twins are also present in Zr_2Cu and τ_5 phases.

The DSC profiles of heating and cooling runs are shown in Fig. 4(a) and (b), respectively. For the binary $Zr_{50}Cu_{50}$ (0Al) transformation temperatures were determined to be $M_s = 446$ K, $M_f = 342$ K, $A_s = 537$ K and $A_f = 552$ K (M_f: forward martensitic transformation finish temperature; A_f: reverse martensitic transformation finish temperature). Two-step transformation behaviors are present in 0Al during forward martensitic transformation (indicated by arrows in Fig. 4(b)), which were previously observed by Firstov et al. [9], who attributed them to the transformation from B2 to B19′ and then to Cm phases on cooling. This two-step transformation is absent in reverse MT, which is probably due to by the overlap of two peaks [9]. Same behaviors occur in 2Al and 4Al. For the 2Al sample, the reverse MT starts at 505 K and finishes at around 520 K on heating, and the forward MT starts at 415 K and finishes at around 310 K on cooling. The M_s decreases to 362 K as Al content is up to 4 mol%, and $A_s = 474$ K. DSC curves in Fig. 4(a) show that the reverse MT temperatures in 6Al are almost same with that in 4Al, but the forward MT shifts to lower temperature with $M_s = 311$ K and $M_f = 242$ K. As the Al addition up to 8, 10 mol%, the reverse MT temperatures increase slightly, and the forward MT temperatures are almost same with that in 6Al. Simultaneously, the height of the endothermic peaks in reverse MT and exothermic peaks in forward MT decreases with the increase in Al content, and the tendency is more pronounced in sample with $x > 6$, which is induced by the decrease in the volume fraction of ZrCu phase caused by more formation of Zr_2Cu and τ_5 as shown in Fig. 2. The DSC curves are almost flat in 10Al. The measured MT temperatures are plotted as a function of overall Al content of the alloys in Fig. 5(a). It was found that the changes in M_s, M_f, A_s, and A_f exhibit two stages. In the first stage, all the transformation temperatures decrease monotonically with the overall Al content, and almost constant hysteresis ($\Delta T = A_s - M_s$) around 90 K for the range $0 \leq x < 6$. The transformation hysteresis increases to ~150 K as Al content up to 6 mol%. As shown in Fig. 5(a), M_s and A_s are more or less constant as $x \geq 6$, especially M_s. The finish temperatures in forward MT are not given because the forward MT cannot undergoes completely in 8Al and 10Al. However, A_f shows increasing trend as $x \geq 6$, and thus the reverse transformation temperature interval ΔA ($=A_f - A_s$) increases, leading to the large hysteresis. For $x < 4$ samples, M_s and M_f are higher than room temperature (Fig. 5(a)), therefore, all the B2 structure ZrCu phase transforms to martensite phases, and there is no B2 peaks detected by XRD in the samples with $x = 0, 2$; while for the high Al content samples ($x = 4, 6, 8, 10$), the M_f is lower than room temperature; the forward MT is not carried out completely, and B2 ZrCu phase is partly left in the samples, which is consistent with the XRD analysis. Since the TEM samples are electropolished at 253 K, all the B2 phase completely transformed to martensite. Therefore, B2 phase was not observed under TEM.

In order to further clarify the influence of Al on the MT, we have carried out the EPMA analysis of chemical composition of the ZrCu

phase present in the different alloys (x = 0–10). The measured Zr, Cu and Al contents in the ZrCu phase are plotted in Fig. 5(b) as a function of overall (nominal) Al content of the alloys. It was revealed that the Al content of the ZrCu phase increases significantly with the overall Al content for $0 \leq x < 6$, but the Cu content shows the opposite trend. For $x \geq 6$, both Al and Cu contents remain almost constant, and the Al content saturates at around 5.0 mol%, which is near the solubility limit of Al in the ZrCu phase. However, the Zr content of the ZrCu phase remains constant as the overall Al content increases from 0 to 10 mol%, which indicates that the Al atoms mainly substitute the Cu atoms in the ZrCu phase.

Combining Fig. 5(a) and (b), it can be seen that the variation of M_s also decreases first until x = 6 and remain almost constant as $x > 6$ which is similar with change of Cu content in ZrCu phase. The higher Al content in the ZrCu phase causes lower M_s and A_s until 6 mol%. Thus it is concluded that the substitution of Cu by Al induces the decrease in forward and reverse MT temperatures when the Al addition is less than 6 mol%.

The reason for the increasing A_f observed for the samples with $x > 6$ is not clear, but it can be related to a complex microstructure. In view of the transformation thermodynamics, the transformation temperature interval is a function of elastic strain energy and irreversible energy [24]. It was shown for TiNi [25,26] that the effect of the two non-chemical energy terms can be significant if the grain size is less than 100 nm. The elastic strain energy causes the increase in the forward-transformation temperature intervals as seen in the DSC results (Fig. 4(b)). The irreversible energy is from the introduction of lattice defects during the transformation and leads to a large transformation intervals and a large hysteresis. The high volume fraction of Zr_2Cu and τ_5 phases refines the overall microstructures and it is likely that the more defects and strain are introduced during the transformation. Some of the defects can act as obstacles for the reverse transformation, which lead to a higher A_s and A_f temperature as $x > 6$.

4. Conclusions

The influence of Al content on the martensitic transformation temperature was investigated by differential scanning calorimetry in $Zr_{50}Cu_{50-x}Al_x$ alloys. The substitution of Cu by Al in ZrCu phase leads to a linear decrease in martensitic transformation temperatures until the Al content exceeds the solubility limit in ZrCu phase. X-ray diffraction and transmission electron microscopy observations revealed that the crystallographic structure of ZrCu martensite is predominantly Cm. Higher Al content over 6 mol% results in the formation of Zr_2Cu and τ_5 phases, leading to the complex eutectic microstructures. This may be the cause of the observed increase in transformation interval on heating. The obtained information regarding the composition dependence of martensitic transformation may be useful to design B2/bulk metallic glass composites.

Acknowledgments

This work is partly supported by the Grant-in-Aid for Scientific Research on Innovative Area, “Bulk Nanostructured Metals”, through MEXT, Japan (contract No. 22102004) and also by Iketani Science Foundation. The work was conducted under the inter-university cooperative research program of the Institute for Materials Research, Tohoku University.

References

[1] E.M. Carvalho, I.R. Harris, J. Mater. Sci. 15 (1980) 1224–1230.
[2] Z. Altounian, G.H. Tu, J.O. Strom-Olsen, J. Appl. Phys. 53 (1982) 4755–4760.
[3] A. Inoue, T. Masumoto, N. Yano, J. Mater. Sci. 19 (1984) 3786–3795.
[4] A. Inoue, W. Zhang, Mater. Trans. 45 (2004) 584–587.
[5] Z.W. Zhu, H.F. Zhang, W.S. Sun, B.Z. Ding, Z.Q. Hu, Scr. Mater. 54 (2006) 1145–1149.
[6] Y.N. Koval, G.S. Firstov, A.V. Koto, Scr. Mater. 27 (1992) 1611–1616.
[7] Y.N. Koval, G.S. Firstov, L. Delaey, J.V. Humbeeck, Scr. Metall. Mater. 31 (1994) 799–802.
[8] D. Schryvers, G.S. Firstov, J.W. Seo, J. Van Humbeeck, Y.N. Koval, Scr. Mater. 36 (1997) 1119–1125.
[9] G.S. Firstov, J.V. Humbeeck, Y.N. Koval, J. Phys. IV 11 (2001) 481–486.
[10] J.W. Seo, D. Scheryvers, Acta Mater. 46 (1998) 1165–1175.
[11] G.S. Firstov, J.V. Humbeeck, Y.N. Koval, Mater. Sci. Eng. A 378 (2004) 2–10.
[12] A. Inoue, T. Zhang, T. Masumoto, Mater. Trans. 36 (1995) 391–398.
[13] A. Inoue, W. Zhang, Mater. Trans. 43 (2002) 2921–2925.
[14] Y. Yokoyama, K. Fukaura, A. Inoue, Mater. Sci. Eng. A 375 (2004) 427–431.
[15] A. Inoue, D. Kawase, A.P. Tsai, T. Zhang, T. Masumoto, Mater. Sci. Eng. A 178 (1994) 255–263.
[16] S. Pauly, G. Liu, G. Wang, J. Das, K.B. Kim, U. Kuhn, D.H. Kim, J. Eckert, Appl. Phys. Lett. 95 (2009) 101906.
[17] S. Pauly, J. Das, J. Bednarcik, N. Mattern, K.B. Kim, D.H. Kim, J. Eckert, Scr. Mater. 60 (2009) 431–434.
[18] S. Pauly, G. Liu, G. Wang, U. Kühn, N. Mattern, J. Eckert, Acta Mater. 57 (2009) 5445–5453.
[19] J. Das, S. Pauly, M. Bostrom, K. Durst, M. Goken, J. Eckert, J. Alloys Compd. 483 (2009) 97–101.
[20] S. Pauly, S. Gorantla, G. Wang, U. Kühn, J. Eckert, Nat. Mater. 9 (2010) 473–477.
[21] L.Q. Xing, P. Ochin, J. Bigot, J. Non-cryst. Solids 205 (1996) 637–640.
[22] A. Slebarski, M. Hafez, W. Zarek, Solid State Commun. 82 (1992) 59–61.
[23] V.Y. Markiv, V.V. Burnashova, Poroshk. Metall. 12 (1970) 53–58.
[24] H.C. Tong, C.M. Wayman, Acta Metall. 22 (1974) 887–896.
[25] K. Tsuchiya, M. Ohnuma, K. Nakajima, T. Koike, Y. Todaka, M. Umemoto, Mater. Res. Soc. Symp. Proc., vol. 1129-V12-01.
[26] T. Waitz, V. Kazykhanov, H.P. Karnthaler, Acta Mater. 52 (2004) 137–147.